The Journal of Engineering

The 9th International Conference on Power Electronics, Machines and Drives (PEMD 2018)

IET Journals
The Institution of Engineering and Technology

Control and operation of the MMC-based drive with reduced capacitor voltage fluctuations

eISSN 2051-3305
Received on 22nd June 2018
Accepted on 31st July 2018
E-First on 4th April 2019
doi: 10.1049/joe.2018.8080
www.ietdl.org

Mauricio Antonio Espinoza Bolaños[1] ✉, Matías Díaz[2], Felipe Donoso[3], Arturo Letelier[3], Roberto Cárdenas[3]

[1]*Department of Electrical Engineering, University of Costa Rica, San José, Costa Rica*
[2]*Department of Electrical Engineering, University of Santiago of Chile, Santiago, Chile*
[3]*Department of Electrical Engineering, University of Chile, Santiago, Chile*
✉ *E-mail: mauricio.espinoza_bola@ucr.ac.cr*

Abstract: The modular multilevel converter (MMC) has emerged as a suitable topology for high power drive applications. However, the voltage fluctuations of its floating capacitors increase the control complexity of the converter. In this study, the MMC dc-port voltage is manipulated to regulate the amplitude of these fluctuations to a constant value during the whole frequency range. The proposed approach has several advantages when compared with the conventional ones since it minimises the voltage fluctuation in the capacitor cells. Additionally, it decreases the common-mode voltage at low frequencies and the capacitor rms current, increasing their expected lifespan and reducing the winding insulation damages and the leakage currents in the bearing of the machine. The effectiveness of the proposed control strategy is validated with a laboratory-based prototype composed of 18 power cells, feeding a vector-controlled induction machine.

1 Introduction

Since the invention of the modular multilevel converter (MMC), this topology has been proposed for applications such as rail train [1], high-voltage dc transmission (HVDC) [2] and machine drives [3–16]. Although the MMC has several advantages over others high power modular converters (mainly for quadratic torque-speed profile loads [3, 4]), significant efforts are still required to improve its performance for drive applications. The MMC topology is shown in Fig. 1. The converter is composed of six 'clusters' connected to form an ac port that feeds the machine and a dc port. Each cluster has an inductor L and n cascaded half-bridge modules. The energy in each cell is stored by a 'flying' capacitor C. Consequently, the proper operation of the MMC-based drive requires a control system to maintain the capacitor voltage balanced. This target is complex to achieve when the machine is operating at low speed because large voltage fluctuations occur in the capacitors. For this reason, in the so-called 'low-frequency mode' (LFM), mitigating variables (circulating currents and common-mode voltage) are used to reduce the voltage fluctuations, maintaining them within an acceptable margin [7, 8, 13, 17]. On the other hand, when the mitigating signals are no longer required, the 'high-frequency mode' (HFM) is enabled.

As is well known, the lifetime of electrolytic capacitors is nominally below semiconductors lifetime. Regarding reliability, this fact represents a significant drawback of MMC family because its capacitors are always subjected to voltage fluctuations. In consequence, several control strategies have been proposed to decrease the voltage capacitor oscillations. Another approach is developing new dielectric material capacitors, such as film capacitors, to extend the lifespan of cell capacitors, and there is an important ongoing research being carried out and new material capacitors, such as film capacitors, represent an excellent alternative to extending the lifetime of the cell capacitors [18, 19].

A novel control system for the MMC-based drive is proposed to solve the problems mentioned above. This new control scheme considers the manipulation of the dc-port voltage as a function of the capacitor voltage fluctuations. The major advantage of this methodology is that the capacitor voltage fluctuations are regulated within a pre-defined margin during the whole frequency range. Accordingly, contrary to the conventional approaches, the amplitude of the capacitor fluctuations is not dependent on the machine frequency, and it can be minimised as much as possible, reducing the rms current in the capacitors and increasing their expected lifespan. What is more, this work shows that the common-mode voltage and circulating currents are reduced at the start-up of the machine when the dc-port voltage is regulated as proposed, eliminating problems such as winding insulation damages, leakage currents in the bearing etc.

The remainder of this paper is organised as follows. The modelling and analysis of the MMC-based drive is discussed in Section 2, while the effect of applying a dynamic dc-port voltage to the MMC-based drive is discussed in Section 3. Several experimental results are presented in Section 4 by using a vector-controlled induction machine being fed by a MMC in the whole

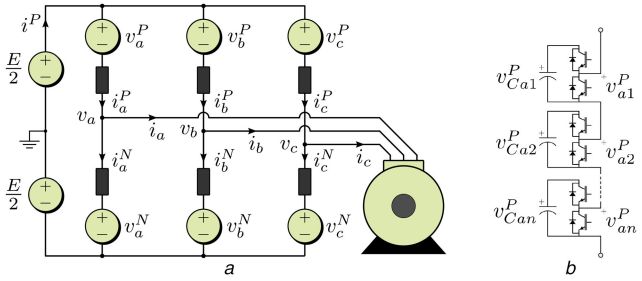

Fig. 1 *MMC-based drive*
(a) Converter topology. (b) Cluster

frequency range, including start-up and zero-crossing speed. Finally, Section 5 presents the conclusions of this work.

2 Dynamic modelling and analysis of the MMC

Recently, a modelling approach for the MMC has been reported in [12, 14]. In these papers, the $\Sigma\Delta\alpha\beta 0$- transformation is used to represent the cluster currents and total capacitor voltages (the sum of the capacitor voltages in a cluster) into a new coordinate system, allowing a decoupled control of each variable. To perform this modelling, the dynamics of these signals are derived as follows (see Fig. 1):

$$L\frac{\mathrm{d}}{\mathrm{d}t}\overbrace{\begin{bmatrix} i_a^P & i_b^P & i_c^P \\ i_a^N & i_b^N & i_c^N \end{bmatrix}}^{:=\mathbf{I}_{abc}^{PN}} = -\overbrace{\begin{bmatrix} v_a^P & v_b^P & v_c^P \\ v_a^N & v_b^N & v_c^N \end{bmatrix}}^{:=\mathbf{V}_{abc}^{PN}} - \frac{E}{2}+\begin{bmatrix} 1 & 1 & 1 \\ 1 & 1 & 1 \end{bmatrix} + \begin{bmatrix} -v_a & -v_b & -v_c \\ v_a & v_b & v_c \end{bmatrix} \tag{1}$$

$$C\bar{v}_C\frac{\mathrm{d}}{\mathrm{d}t}\underbrace{\begin{bmatrix} v_{Ca}^P & v_{Cb}^P & v_{Cc}^P \\ v_{Ca}^N & v_{Cb}^N & v_{Cc}^N \end{bmatrix}}_{:=\mathbf{V}_{abc}^{PN}} \simeq \underbrace{\begin{bmatrix} p_a^P & p_b^P & p_c^P \\ p_a^N & p_b^N & p_c^N \end{bmatrix}}_{:=\mathbf{P}_{abc}^{PN}}, \tag{2}$$

where $\bar{v}_C$ is the algebraic mean value of the voltage in all capacitors of the MMC, $p_a^P = i_a^P v_a^P$, $p_b^P = i_b^P v_b^P$, etc., are the cluster power flows and

$$v_{Ca}^P = v_{Ca1}^P + v_{Ca2}^P + \cdots + v_{Can}^P,\ v_{Ca}^N = v_{Ca1}^N + v_{Ca2}^N + \cdots + v_{Can}^N,$$

etc., are the total cluster voltages. Expression (1) is based on Kirchhoff's voltage law applied into the converter depicted in Fig. 1. On the other hand, (2) denotes the energy balance in the MMC clusters, assuming that the total cluster voltages are close to an operating point, as is in a well-controlled MMC.

As discussed before, to achieve a decoupled control of the converter currents and voltages, the $\Sigma\Delta\alpha\beta 0$- transformation is utilised. This transformation is given by

$$\boldsymbol{X}_{\alpha\beta 0}^{\Sigma\Delta} := \boldsymbol{C}^{\Sigma\Delta}\cdot\boldsymbol{X}_{abc}^{PN}\cdot\boldsymbol{C}_{\alpha\beta 0}^{T} \tag{3}$$

where $\boldsymbol{X}_{abc}^{PN}$ represents the matrix to be transformed (e.g. I_{abc}^{PN} or V_{abc}^{PN}) and the matrices $\boldsymbol{C}^{\Sigma\Delta}$ and $\boldsymbol{C}_{\alpha\beta 0}^{T}$ are

$$\boldsymbol{C}^{\Sigma\Delta} = \begin{bmatrix} \frac{1}{2} & \frac{1}{2} \\ 1 & -1 \end{bmatrix},\ \boldsymbol{C}_{\alpha\beta 0}^{T} = \begin{bmatrix} \frac{2}{3} & \frac{-1}{3} & \frac{-1}{3} \\ 0 & \frac{1}{\sqrt{3}} & \frac{-1}{\sqrt{3}} \\ \frac{1}{3} & \frac{1}{3} & \frac{1}{3} \end{bmatrix}^{\mathrm{T}} \tag{4}$$

Hence, applying (3) to (1) and (2) and simplifying leads to

$$L\frac{\mathrm{d}}{\mathrm{d}t}\overbrace{\begin{bmatrix} i_\alpha^\Sigma & i_\beta^\Sigma & \frac{1}{3}i^P \\ i_\alpha & i_\beta & 0 \end{bmatrix}}^{:=\mathbf{I}_{\alpha\beta 0}^{\Sigma\Delta}} = -\overbrace{\begin{bmatrix} v_\alpha^\Sigma & v_\beta^\Sigma & v_0^\Sigma \\ v_\alpha^\Delta & v_\beta^\Delta & v_0^\Delta \end{bmatrix}}^{:=\mathbf{V}_{\alpha\beta 0}^{\Sigma\Delta}} - 2\begin{bmatrix} 0 & 0 & -\frac{1}{4}E \\ v_\alpha & v_\beta & v_0 \end{bmatrix} \tag{5}$$

$$C\bar{v}_C\frac{\mathrm{d}}{\mathrm{d}t}\underbrace{\begin{bmatrix} v_{C\alpha}^\Sigma & v_{C\beta}^\Sigma & v_{C0}^\Sigma \\ v_{C\alpha}^\Delta & v_{C\beta}^\Delta & v_{C0}^\Delta \end{bmatrix}}_{:=\mathbf{V}_{C\alpha\beta 0}^{\Sigma\Delta}} \simeq \underbrace{\begin{bmatrix} p_\alpha^\Sigma & p_\beta^\Sigma & p_0^\Sigma \\ p_\alpha^\Delta & p_\beta^\Delta & p_0^\Delta \end{bmatrix}}_{:=\mathbf{P}_{\alpha\beta 0}^{\Sigma\Delta}}, \tag{6}$$

where the machine currents (i_α and i_β) and voltages (v_α, v_β and v_0) are expressed in $\alpha\beta 0$-coordinates, i_α^Σ and i_β^Σ are the circulating currents and i^P is the dc-port current. Based on (5), each current can be easily controlled manipulating only one voltage in the matrix $\boldsymbol{V}_{\alpha\beta 0}^{\Sigma\Delta}$, achieving a decoupled control.

As discussed in [14], the vector representation of (6) improves the implementation of high-dynamic control strategies using vector control algorithms. Specifically, defining the power flows and the total cluster voltages as vectors (e.g. $\mathbf{p}_{\alpha\beta}^\Sigma = p_\alpha^\Sigma + \mathrm{j}p_\beta^\Sigma$, $\boldsymbol{v}_{C\alpha\beta}^\Sigma = v_{C\alpha}^\Sigma + \mathrm{j}v_{C\beta}^\Sigma$, etc), the vector model of (6) is obtained as (see [14] and Appendix A for details):

$$C\bar{v}_C\frac{\mathrm{d}\boldsymbol{v}_{C\alpha\beta}^\Sigma}{\mathrm{d}t} \simeq \mathbf{p}_{\alpha\beta}^\Sigma \simeq \frac{1}{2}E\mathbf{i}_{\alpha\beta}^\Sigma - \frac{1}{4}(\mathbf{i}_{\alpha\beta}\boldsymbol{v}_{\alpha\beta})^{\mathrm{c}} - \frac{1}{2}v_0\mathbf{i}_{\alpha\beta} \tag{7a}$$

$$C\bar{v}_C\frac{\mathrm{d}\boldsymbol{v}_{C\alpha\beta}^\Delta}{\mathrm{d}t} \simeq \mathbf{p}_{\alpha\beta}^\Delta \simeq \frac{1}{2}E\mathbf{i}_{\alpha\beta} - \frac{2}{3}i^P\boldsymbol{v}_{\alpha\beta} - (\boldsymbol{v}_{\alpha\beta}\mathbf{i}_{\alpha\beta}^\Sigma)^{\mathrm{c}} - 2v_0\mathbf{i}_{\alpha\beta}^\Sigma \tag{7b}$$

$$C\bar{v}_C\frac{\mathrm{d}v_{C0}^\Sigma}{\mathrm{d}t} \simeq p_0^\Sigma \simeq \frac{1}{6}Ei^P - \frac{1}{4}\Re\left[\boldsymbol{v}_{\alpha\beta}(\mathbf{i}_{\alpha\beta})^{\mathrm{c}}\right] \tag{7c}$$

$$C\bar{v}_C\frac{\mathrm{d}v_{C0}^\Delta}{\mathrm{d}t} \simeq p_0^\Delta \simeq -\Re\left[\boldsymbol{v}_{\alpha\beta}(\mathbf{i}_{\alpha\beta}^\Sigma)^{c}\right] - \frac{2}{3}i^P v_0 \tag{7d}$$

where the superscript 'c' stands for the complex conjugated operator.

For a proper operation of the MMC, the oscillations of the total cluster voltages (indicated by the super-script '$\sim$') have to be within an acceptable value. In previous works it has been shown that the term $\tilde{v}_{C\alpha\beta}^\Delta$ produces a fundamental ω_e fluctuation, which amplitude is proportional to ω_e^{-1}, $\tilde{v}_{C\alpha\beta}^\Delta$ produces a double frequency oscillation and $\tilde{v}_{C0}^\Sigma$, as well as $\tilde{v}_{C0}^\Sigma$, do not produce fluctuations in the MMC capacitors. It straightforward to demonstrate setting the signals $\mathbf{i}_{\alpha\beta}^\Sigma$ and v_0 to zero and integrating (7a)–(7d), resulting in

$$\tilde{\boldsymbol{v}}_{C\alpha\beta}^\Sigma \simeq \frac{-1}{\mathrm{j}8\omega_e C\bar{v}_C}(\mathbf{i}_{\alpha\beta}\boldsymbol{v}_{\alpha\beta})^{\mathrm{c}} \tag{8a}$$

$$\tilde{\boldsymbol{v}}_{C\alpha\beta}^\Delta \simeq \frac{1}{\mathrm{j}\omega_e C\bar{v}_C}\left(\frac{1}{2}E\mathbf{i}_{\alpha\beta} - \frac{2}{3}i^P\boldsymbol{v}_{\alpha\beta}\right) \tag{8b}$$

$$\tilde{v}_{C0}^\Sigma \simeq n\tilde{v}_C,\quad \tilde{v}_{C0}^\Sigma \simeq 0 \tag{8c}$$

Based on the inverse $\Sigma\Delta\alpha\beta 0$-transformation, the total capacitor voltages in $P\ N\ abc$ coordinates can be expressed using the vector voltages of (6). For example, the voltages v_{Ca}^P and v_{Ca}^N are expressed as follows:

$$v_{Ca}^P = \frac{1}{2}\Re[v_{C\alpha\beta}^\Delta] + \Re[v_{C\alpha\beta}^\Sigma] + \frac{1}{2}v_{C0}^\Delta + v_{C0}^\Sigma \tag{9a}$$

$$v_{Ca}^N = \frac{1}{2}\Re[v_{C\alpha\beta}^\Delta] + \Re[v_{C\alpha\beta}^\Sigma] - \frac{1}{2}v_{C0}^\Delta + v_{C0}^\Sigma \tag{9b}$$

Consequently, the maximum amplitude of the oscillating component of the total cluster voltages, $\left|\tilde{v}_{Cx}^X\right|$, can be approximated with the vector voltages $\boldsymbol{v}_{C\alpha\beta}^\Delta$ and $\boldsymbol{v}_{C\alpha\beta}^\Sigma$ as follows:

$$\left|\tilde{v}_{Cx}^X\right| \simeq \frac{1}{2}\|\ \boldsymbol{v}_{C\alpha\beta}^\Delta\ \| + \|\ \boldsymbol{v}_{C\alpha\beta}^\Sigma\ \| \tag{10}$$

where $x = \{a, b, c\}$ and $X = \{P, N\}$. Notice that (10) represents the worst case situation for $\left|\tilde{v}_{Cx}^X\right|$, since the amplitude of $\boldsymbol{v}_{C\alpha\beta}^\Delta$ and $\boldsymbol{v}_{C\alpha\beta}^\Sigma$ are summed.

3 Influence of the dc-port voltage E in the MMC electrical variables

In this paper, a new control methodology is proposed to operate the MMC as a machine drive. This strategy manipulates the dc-port voltage E to maintain the fluctuations of the total cluster voltages

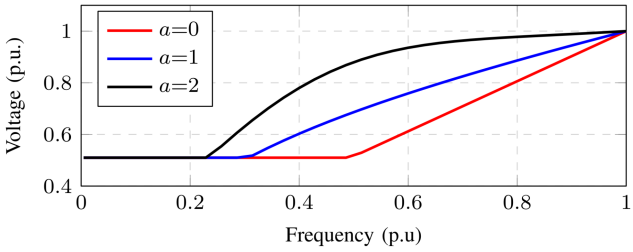

Fig. 2 *Required value of the voltage E to regulate* $|\tilde{v}_{Cx}^{X}|$ *to a constant value*

within a voltage margin in the whole frequency range. The effect of modifying the dc-port voltage E is analysed below.

3.1 During low-frequency mode

In the LFM circulating currents and common-mode voltage are needed to maintain the fluctuations of the vector voltage $\boldsymbol{v}_{C\alpha\beta}^{\Delta}$ within an acceptable value. Due to its oscillating frequency ω_e, it is straightforward to analyse the regulation of $\boldsymbol{v}_{C\alpha\beta}^{\Delta}$ representing (7b) into a dq-coordinate frame rotating at ω_e rad s^{-1} as follows:

$$C\bar{v}_C\frac{\mathrm{d}\boldsymbol{v}_{Cdq}^{\Delta}}{\mathrm{d}t} \simeq \underbrace{\tfrac{1}{2}E\mathbf{i}_{dq} - \tfrac{2}{3}i^{P}\boldsymbol{v}_{dq}}_{:=\mathbf{P}\omega_e} - \underbrace{\mathrm{j}C\bar{v}_C\omega_e\boldsymbol{v}_{Cdq}^{\Delta}}_{:=\mathbf{P}m} - \underbrace{2v_0\mathbf{i}_{dq}^{\Sigma}}_{:=\mathbf{P}c} \tag{11}$$

Considering ideal conditions, the set-point values of $\tilde{\mathbf{i}}_{\alpha\beta}^{\Sigma}$ and $\tilde{v}_0$ can be defined as

$$\tilde{\mathbf{i}}_{dq}^{\Sigma *} = \frac{1}{2V_0}(\mathbf{p}_{\omega e} - \mathbf{p}_m)f(t), \tag{12}$$

$$\tilde{v}_0^{*} = V_0\mathrm{sign}[f(t)] \tag{13}$$

where V_0 is the amplitude of the common-mode voltage. Consequently, the power term $\mathbf{p}_c$ can be expressed as:

$$\mathbf{p}_c = (\mathbf{p}_{\omega_e} - \mathbf{p}_m)|f(t)| \tag{14}$$

Hence, $\mathbf{p}\omega_e$ and $\mathbf{p}_m$ are eliminated from (11) if $f(t)$ is a high frequency signal compared to ω_e during LFM, such that the mean value of $|f(t)| = 1$ (considering one period of $f(t)$ see [7, 8, 13]). Notice that if $\mathbf{p}_m$ is defined as a non-zero vector (i.e. a fundamental oscillation is allowed in $\boldsymbol{v}_{C\alpha\beta}^{\Delta}$) the circulating currents decrease as the machine frequency increases [see $\mathbf{p}_m$ in (11)]. A discussion regarding this methodology is addressed in [20].

Based on (12), it is concluded that the mitigating circulating currents are inversely proportional to V_0. Neglecting the inductor voltage drop and considering that the output cluster voltages has to be positive, it is straightforward to demonstrate that the maximum amplitude of the common-mode voltage can be approximated as [see (1)]:

$$V_0 \simeq \frac{1}{2}E - \parallel \mathbf{v}_{dq} \parallel \tag{15}$$

where $\mathbf{v}_{dq}$ is the machine voltage in a dq-rotating frame. At the machine start-up, $\omega_e \simeq 0\,\mathrm{rads}^{-1}$ and $\parallel \mathbf{v}_{dq} \parallel \simeq 0\,\mathrm{V}$; therefore, $\tilde{\mathbf{i}}_{dq}^{\Sigma *}$ and $\tilde{v}_0^{*}$ as defined in (12) and (13) results in:

$$\tilde{\mathbf{i}}_{dq}^{\Sigma *}(\omega_e \simeq 0) \simeq \mathbf{i}_{dq}f(t), \tag{16}$$

$$V_0(\omega_e \simeq 0) \simeq \frac{1}{2}E \tag{17}$$

The importance of this result is that the amplitude of the circulating currents is not affected by variations in the dc-port voltage E or the voltage $\boldsymbol{v}_{C\alpha\beta}^{\Delta}$ during the machine start-up. However, the amplitude of the common-mode voltage is modified at the same ratio of the dc-port voltage. In this manner, it is an attractive solution to maintain a low value of the dc-port voltage during the LFM to reduce the required common-mode voltage to eliminate the high-voltage fluctuations in the MMC capacitors.

3.2 During high-frequency mode

The voltage E cannot be maintained in a low value during the whole frequency range because the output cluster voltage would reach negative values as ω_e increases. For this reason, E has to be manipulated from its minimum value in LFM, $E_{\min}$, until its maximum/nominal value in HFM, $E_{\max}$.

In this paper, a simple method to achieve this task is proposed. What is more, the presented methodology ensures a constant voltage fluctuation in the total cluster voltages during the HFM. Of all the possible values for this fluctuation, the minimum value is preferred since it increases the lifespan of the MMC capacitors. Consequently, the value of $|\tilde{v}_{Cx}^{X*}|$ can be determined using (10) for the nominal machine conditions.

From (11), the HFM is enable when $\parallel \mathbf{p}_c \parallel \simeq 0$ (i.e. the mitigating variables are no longer required to reduce the voltage fluctuations of $\boldsymbol{v}_{C\alpha\beta}^{\Delta}$). Therefore, in steady-state conditions $\mathbf{p}\omega_e = \mathbf{p}_m$. Supposing that the MMC is balanced (i.e. $\boldsymbol{v}_{C\alpha\beta}^{\Sigma} = \tilde{\boldsymbol{v}}_{C\alpha\beta}^{\Sigma}$ and $i^{P} \simeq \frac{3}{2E}\Re\{\boldsymbol{v}_{dq}i_{dq}^{c}\}$), the amplitude of the power fluctuations $\mathbf{p}\omega_e$ and $\mathbf{p}_m$ can be expressed as follows:

$$\parallel \mathbf{p}_{\omega e}(E) \parallel = \parallel \frac{1}{2}E\mathbf{i}_{\mathrm{dq}} - \Re\{\mathbf{v}_{\mathrm{dq}}\mathbf{i}_{\mathrm{dq}}^{\mathrm{c}}\}\frac{\mathbf{v}_{dq}}{E} \parallel \tag{18}$$

$$\parallel \mathbf{p}_m\left(|\tilde{v}_{Cx}^{X*}|\right) \parallel = 2C\bar{v}_C\omega_e\left(|\tilde{v}_{Cx}^{X*}| - \parallel \boldsymbol{v}_{C\alpha\beta}^{\Sigma} \parallel\right) \tag{19}$$

where $\parallel \boldsymbol{v}_{C\alpha\beta}^{\Sigma} \parallel = \parallel \boldsymbol{v}_{C\alpha\beta}^{\Delta} \parallel$ has been written as a function of $\parallel \boldsymbol{v}_{C\alpha\beta}^{\Sigma} \parallel$ and $|\tilde{v}_{Cx}^{X*}|$ by using (10). Finally, based on (18) and (19), it can be concluded that the dc-port voltage E can be manipulated to achieve a desired value of $|\tilde{v}_{Cx}^{X}|$, $|\tilde{v}_{Cx}^{X*}|$.

Fig. 2 shows the dc-port voltage E as a function of ω_e to achieve the minimum value of $|\tilde{v}_{Cx}^{X}|$ during the whole frequency range in an MMC as the one utilised in the experimental results of this paper. In the figure, the electrical torque was defined as

$$T_{\mathrm{e}}(\omega_e) = T_{e0} + (T_{e\mathrm{Nom}} - T_{e0})\left(\frac{\omega_e}{\omega_{e\mathrm{Nom}}}\right)^{a} \tag{20}$$

where T_{e0} is the starting-torque, $T_{e\mathrm{Nom}}$ is the nominal torque, $\omega_{e\mathrm{Nom}}$ is nominal machine frequency and a is a parameter to define the machine torque-speed profile.

4 Experimental results and setup

Experimental results of the proposed control methodology have been obtained using an 18-power cell MMC-based drive. The experimental setup is shown in Fig. 3, while its parameters are given in Table 1. The MMC is driving a 7.5 kW vector-controlled induction machine connected to a permanent magnet generator

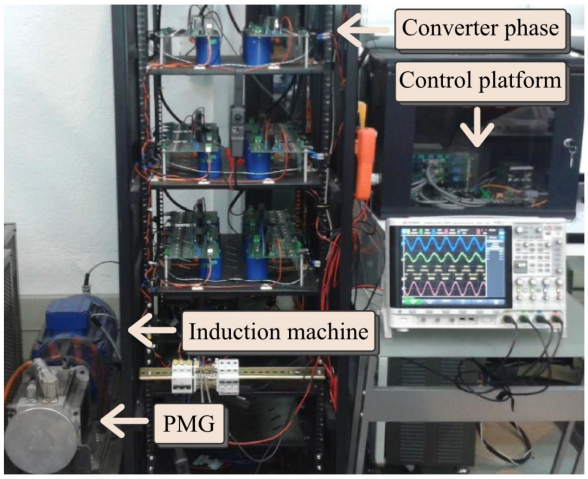

Fig. 3 *Photograph of the laboratory experimental system*

Table 1 Set-up parameters for the 18 cells MMC-drive

Parameter	Symbol	Value	Unit
dc-port voltage	E	450	V
cluster inductor	L	2,5	mH
cell capacitor	C	4700	μF
cell dc voltage	v_C^*	150	V
switching frequency per cell	f_s	5000	Hz

(PMG). A resistor bank has been connected to the PMG output providing a 4 kW load at nominal speed. Hall-effect transducers are used to measure the dc-port voltage, the capacitor voltages and the cluster currents. To control the system, a platform based on two field-programmable gate array boards (Actel ProASIC3) and a digital signal processor (TI TMS320C6713) is used. A programmable AMETEK power supply model CSW5550 generates the dc-port voltage as discussed in Section 3. In a commercial implementation, this voltage can be generated using a medium voltage source as those presented in [21, 22] or another MMC with full-bridge cells [23, 24].

Considering that the contribution of this paper is to analyse and show the effect of a dynamic variation of the dc-port voltage in the MMC-based drive, the converter cluster voltages and machine currents have been controlled by using conventional control strategies [12, 14, 20]. The vector voltage $\boldsymbol{v}_{C\alpha\beta}^{\Delta}$ is regulated in a dq-rotating frame during LFM. This task is carried out by using an ac-component in the circulating currents that creates a power flow with the common-mode voltage [see the term $-2v_0 i_{\alpha\beta}^{\Sigma}$ in (11)]. During HFM, this ac-component creates a power flow with the machine voltages to regulate $\boldsymbol{v}_{C\alpha\beta}^{\Delta}$ [see the term $(\boldsymbol{v}_{\alpha\beta} i_{\alpha\beta}^{\Sigma})^c$ in (7b)]. Additionally, the vector voltage $\boldsymbol{v}_{C\alpha\beta}^{\Sigma}$ is controlled by adding a dc-component in the circulating currents for both, low- and high-frequency modes to manipulate the power flow $(1/2)E\mathbf{i}_{\alpha\beta}^{\Sigma}$ in (7a). On the other hand, the dc-port current i^P is manipulated during LFM to regulate v_{C0}^{Δ} by using an ac-component in-phase with the common-mode voltage [see (7d)]. In HFM, the power flow $-\Re[\boldsymbol{v}_{\alpha\beta}(\mathbf{i}_{\alpha\beta}^{\Sigma})^c]$ in (7d) regulates v_{C0}^{Δ}. A complete description of the control diagrams utilised in this work can be found in [12, 14, 20].

Fig. 4 depicts the dynamic performance when the MMC drives the induction machine from 0 to 2000 rpm for constant (left) and manipulated (right) dc-port voltage. The speed profile for both test is shown in Figs. 4*a* and *b*. Notice that this profile includes the machine start-up and the zero-crossing condition, what represents the worst case situation for an MMC-based drive. The machine currents are shown in Figs. 4*c* and *d*, demonstrating that the same mechanical load was applied during the tests.

The dc-port voltage (blue line) and the desired output voltage of a cluster (red line) are depicted in Figs. 4*e* and *f*. As shown, the MMC cluster has to synthesise a high common-mode voltage during the LFM because the nominal dc-port voltage is applied during the machine operation. This is concluded based on the high-frequency signals of the output cluster voltage at low-frequencies [see (17)]. However, the required common-mode voltage is naturally lower when the dc-port voltage is reduced as in Fig. 4*f*. Notice that in these experimental results, the voltage E was regulated to a 50% of its nominal value in LFM, which represent a feasible reduction for the aforementioned input converters [21–24].

The total cluster voltages are shown in Figs. 4*g* and *h*. As discussed in Section 3, a margin-based control strategy maintains their amplitudes constant during LFM [20]. Notice that their peak-to-peak value for a constant dc-port voltage is 40 V; however, it is possible to reduce this fluctuation to 20 V peak-to-peak applying a manipulated dc-port voltage, increasing the expected lifespan of the capacitor cells and decreasing their rms current [23]. What is more, this amplitude is maintained constant by manipulating E as the machine speed increases in HFM. Figs. 4*i* and *j* depict the obtained circulating currents during these tests. It is important to mention that the peak value of both currents is similar, and then the converter current rating has not to be increased when the proposed strategy is implemented, as demonstrated in Figs. 4*k* and *l*, where it is shown that the cluster currents have a similar peak-value for both tests.

5 Conclusions

This paper has demonstrated that the dc-port voltage of an MMC can be manipulated to maintain constant the amplitude of the capacitor voltage fluctuations in drive applications. It has been shown that this methodology allows a reduction in both, the rms current and voltage fluctuation of the capacitor cells, increasing its expected lifespan. Additionally, a low common-mode voltage at the machine start-up is required since the dc-port voltage is reduced with the proposed scheme; therefore, problems such as winding insulation damages, leakage currents in the bearing etc. are also minimised.

Extensive experimental results for a laboratory prototype have been presented in this work. Dynamic experiments in both operating modes (high- and low-frequency modes) have been realised and thoroughly discussed. The performance considering ramp variations in the speed and zero-crossing speed transitions have been experimentally investigated and good performance has

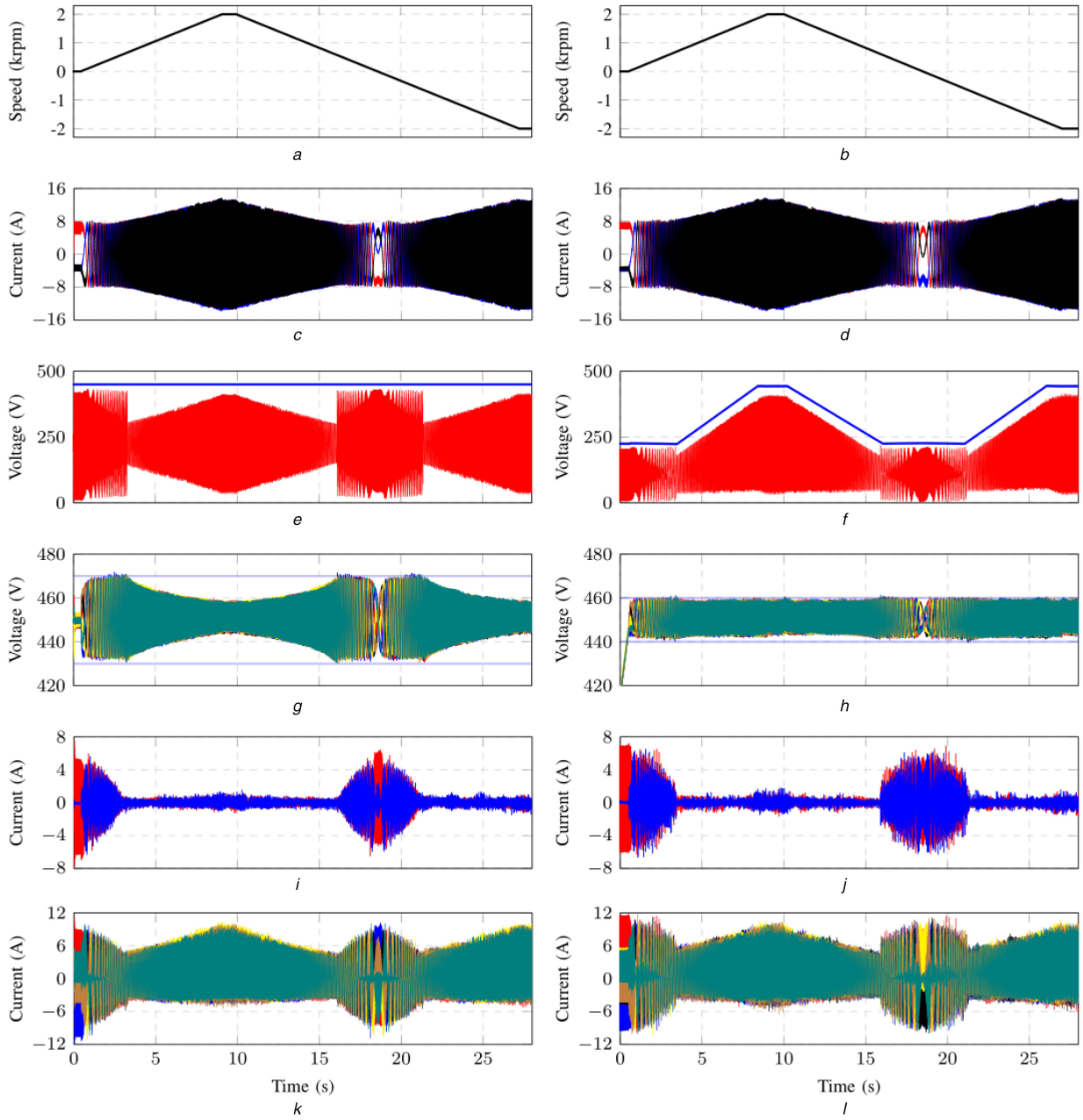

Fig. 4 *Comparison of the dynamic performance of the MMC-based drive for constant (left) and manipulated (right) dc-port voltage.*
(a)–(b) Machine speed, ***(c)–(d)*** Machine currents, ***(e)–(f)*** dc-port voltage E (blue line) and desired output cluster voltage (red), ***(g)–(h)*** Total cluster voltages, ***(i)–(j)*** Circulating currents, ***(k)–(l)*** Cluster currents

been demonstrated. The experimental results have demonstrated the effectiveness of the proposed strategies.

6 Acknowledgments

The support of Fondecyt grant no. 1140337 and the AC3E, Basal Project FB0008 is kindly acknowledged. Additionally, the funding provided by CONICYT-PCHA/Doctorado Nacional/ 2014-63140233 and the University of Costa Rica is also recognised.

7 References

[1] Marquardt, R.: 'Stromrichterschaltungen mit verteilten energiespeichern'. German Patent DE20 122 923 U1, 2001

[2] Siemens: 'HVDC PLUS – basics and principle of operation', 2013. Available at http://www.energy.siemens.com/br/pool/br/transmissao-de-energia/transformadores/hvdc-plus-basics-and-principle-of-operation.pdf

[3] Okazaki, Y., Kawamura, W., Hagiwara, M., *et al.*: 'Experimental comparisons between modular multilevel DSCC inverters and TSBC converters for medium-voltage motor drives', *IEEE Trans. Power Electron.*, 2016, **PP**, (99), pp. 1–1

[4] Ilves, K., Bessegato, L., Norrga, S.: 'Comparison of cascaded multilevel converter topologies for AC/AC conversion'. 2014 Int. Power Electronics Conf. (IPEC-Hiroshima 2014 – ECCE-ASIA), Hiroshima, Japan, May. 2014, pp. 1087–1094

[5] Hagiwara, M., Nishimura, K., Akagi, H.: 'A medium-voltage motor drive with a modular multilevel PWM inverter', *IEEE Trans. Power Electron.*, 2010, **25**, (7), pp. 1786–1799

[6] Thitichaiworakorn, N., Hagiwara, M., Akagi, H.: 'Experimental verification of a modular multilevel cascade inverter based on double-star bridge cells', *IEEE Trans. Ind. Appl.*, 2014, **50**, (1), pp. 509–519

[7] Hagiwara, M., Hasegawa, I., Akagi, H.: 'Start-up and low-speed operation of an electric motor driven by a modular multilevel cascade inverter', *IEEE Trans. Ind. Appl.*, 2013, **49**, (4), pp. 1556–1565

[8] Korn, A. J., Winkelnkemper, M., Steimer, P.: 'Low output frequency operation of the modular multi-level converter'. 2010 IEEE Energy Conversion Congress and Exposition (ECCE), Atlanta, USA, 12–16 September 2010

[9] Antonopoulos, A., Ängquist, L., Norrga, S., *et al.*: 'Modular multilevel converter AC motor drives with constant torque from zero to nominal speed', *IEEE Trans. Ind. Appl.*, 2014, **50**, (3), pp. 1982–1993

[10] Debnath, S., Qin, J., Bahrani, B., *et al.*: 'Operation, control, and applications of the modular multilevel converter: a review', *IEEE Trans. Power Electron.*, 2015, **30**, (1), pp. 37–53

[11] Antonopoulos, A., Ängquist, L., Harnefors, L., *et al.*: 'Optimal selection of the average capacitor voltage for variable-speed drives with modular

multilevel converters', *IEEE Trans. Power Electron.*, 2015, **30**, (1), pp. 227–234
[12] Kolb, J., Kammerer, F., Gommeringer, M., *et al.*: 'Cascaded control system of the modular multilevel converter for feeding variable-speed drives', *IEEE Trans. Power Electron.*, 2015, **30**, (1), pp. 349–357
[13] Espinoza, M., Espina, E., Diaz, M., *et al.*: 'Improved control strategy of the modular multilevel converter for high power drive applications in low frequency operation'. 2016 18th European Conf. on Power Electronics and Application (EPE), Karlsruhe, Germany, Sep. 2016, pp. 5–9
[14] Espinoza, M., Cárdenas, R., Díaz, M., *et al.*: 'An enhanced *dq*-based vector control system for modular multilevel converters feeding variable-speed drives', *IEEE Trans. Ind. Electron.*, 2017, **64**, (4), pp. 2620–2630
[15] Li, B., Zhou, S., Xu, D., *et al.*: 'An improved circulating current injection method for modular multilevel converters in variable-speed drives', *IEEE Trans. Ind. Electron.*, 2016, **63**, (11), pp. 7215–7225
[16] Siemens: 'SINAMICS SM120 cabinet modules', July 2016. Available at https://www.industry.siemens.com/drives/global/en/converter/mv-drives/Pages/sinamics-sm120-cm.aspx
[17] Li, B., Zhou, S., Xu, D., *et al.*: 'Comparative study of the sinusoidal-wave and square-wave circulating current injection methods for low-frequency operation of the modular multilevel converters'. 2015 IEEE Energy Conversion Congress and Exposition (ECCE), Montreal, Canada, Sep. 2015, pp. 4700–4705
[18] Karanayil, B., Agelidis, V. G., Pou, J.: 'Performance evaluation of three-phase grid-connected photovoltaic inverters using electrolytic or polypropylene film capacitors', *IEEE Trans. Sustain. Energy*, 2014, **5**, (4), pp. 1297–1306, DOI: 10.1109/TSTE.2014.2347967
[19] Wang, H., Blaabjerg, F.: 'Reliability of capacitors for DC link applications in power electronic converters: an overview', *IEEE Trans. Ind. Appl.*, 2014, **50**, (5), pp. 3569–3578, DOI: 10.1109/TIA.2014.2308357
[20] Espinoza, M., Espina, E., Diaz, M., *et al.*: 'Control strategies for modular multilevel converters driving cage machines'. 2017 IEEE 3rd Southern Power Electronics Conf. (SPEC), Puerto Varas, Chile, Diciembre 2017, pp. 1–6
[21] Zhang, M. L., Wu, B., Xiao, Y., *et al.*: 'A multilevel buck converter based rectifier with sinusoidal inputs and unity power factor for medium voltage (4160–7200 V) applications', *IEEE Trans. Power Electron.*, 2002, **17**, (6), pp. 853–863, DOI: 10.1109/TPEL.2002.805600
[22] Abdelsalam, I., Adam, G. P., Holliday, D., *et al.*: 'Single-stage ac-dc buck-boost converter for medium-voltage high-power applications', *IET Renew. Power Gener.*, 2016, **10**, (2), pp. 184–193, DOI: 10.1049/ietrpg.2015.0136
[23] Sau, S., Fernandes, B. G.: 'Modular multilevel converter based variable speed drives with constant capacitor ripple voltage for wide speed range'. IECON 2017 – 43rd Annual Conf. of the IEEE Industrial Electronics Society, Beijing, China, Oct. 2017, pp. 2073–2078, DOI: 10.1109/IECON.2017.8216348
[24] Kumar, Y. S., Poddar, G.: 'Medium-voltage vector control induction motor drive at zero frequency using modular multilevel converter', *IEEE Trans. Ind. Electron.*, 2018, **65**, (1), pp. 125–132, DOI: 10.1109/TIE.2017.2721927

8 Appendix A

8.1 Derivation of the power flows in ΣΔαβ0-coordinates

The power flows of the MMC in $\Sigma\Delta\alpha\beta0$-coordinates are derived in this appendix. Based on the definition of the $\Sigma\Delta\alpha\beta0$-transformation:

$$\mathbf{P}^{\Sigma\Delta}_{\alpha\beta0} = C^{\Sigma\Delta}\cdot\mathbf{P}^{PN}_{abc}\cdot C^{T}_{\alpha\beta0} = C^{\Sigma\Delta}\cdot[\mathbf{V}^{PN}_{abc}\circ\mathbf{I}^{PN}_{abc}]\cdot C^{T}_{\alpha\beta0} \tag{21}$$

where 'o'' denotes the element-by-element multiplication of two matrices. Moreover, the inverse $\Sigma\Delta\alpha\beta0$-transformation of $\boldsymbol{V}^{\Sigma\Delta}_{\alpha\beta0}$ and $\mathbf{I}^{\Sigma\Delta}_{\alpha\beta0}$ is given by

$$\mathbf{V}^{PN}_{abc} = (C^{\Sigma\Delta})^{-1}\cdot\mathbf{V}^{\Sigma\Delta}_{\alpha\beta0}\cdot(C^{T}_{\alpha\beta0})^{-1} \tag{22}$$

$$\mathbf{I}^{PN}_{abc} = (C^{\Sigma\Delta})^{-1}\cdot\mathbf{I}^{\Sigma\Delta}_{\alpha\beta0}\cdot(C^{T}_{\alpha\beta0})^{-1}\cdot \tag{23}$$

$\boldsymbol{V}^{\Sigma\Delta}_{\alpha\beta0}$ is approximated in (5) by neglecting the inductor voltage droop, i.e.:

$$\boldsymbol{V}^{\Sigma\Delta}_{\alpha\beta0} = \begin{bmatrix} v^{\Sigma}_{\alpha} & v^{\Sigma}_{\beta} & v^{\Sigma}_{0} \\ v^{\Delta}_{\alpha} & v^{\Delta}_{\beta} & v^{\Delta}_{0} \end{bmatrix} \simeq 2\begin{bmatrix} 0 & 0 & -\frac{1}{4}E \\ v_{\alpha} & v_{\beta} & v_{0} \end{bmatrix} \tag{24}$$

Finally, inserting (24), (23) and (22) into (21) and rewriting the result in vector form, the power flows of the MMC are derived as those presented in (7a)–(7d).